Skull metastases and osseous venous malformations: the role of diffusion-weighted and dynamic contrast-enhanced MRI

Short title: MRI in distinguishing secondary malignancies

Ryo Kurokawa[a], Mariko Kurokawa[a], Adam Holmes[a], Akira Baba[a], Jayapalli Bapuraj[a], Aristides Capizzano[a], John Kim[a], Ashok Srinivasan[a], and Toshio Moritani[a]

[a] Division of Neuroradiology, Department of Radiology, University of Michigan, 1500 E. Medical Center Dr., Ann Arbor, MI 48109, USA.

* Corresponding author

Ryo Kurokawa, MD, PhD

Division of Neuroradiology, Department of Radiology, University of Michigan, Ann Arbor, Michigan

1500 E Medical Center Dr, UH B2, Ann Arbor, MI 48109.

Email: kuroro63@gmail.com

Phone: +1-784-219-2884 Fax: +1-734-615-9800

This is the author manuscript accepted for publication and has undergone full peer review but has not been through the copyediting, typesetting, pagination and proofreading process, which may lead to differences between this version and the Version of Record. Please cite this article as doi: 10.1111/jon.13034.

Keywords:

skull metastasis; osseous venous malformation; diffusion-weighted imaging; dynamic contrast-enhanced

Funding: This study did not receive specific grants from funding agencies in the public, commercial, or not-for-profit sectors.

Abstract

Background and Purpose

Skull metastasis (SM) is a common secondary malignancy. We evaluated the diagnostic performance of diffusion-weighted imaging (DWI) and dynamic contrast-enhanced magnetic resonance imaging (MRI) in differentiating SM from osseous venous malformations and SM of various origins.

Methods

This study included 31 patients with SM (median age, 64 years; range, 41–87 years; 29 women; 24 and seven patients with breast and non-small cell lung cancer, respectively) and 16 with osseous venous malformations (age, 68 years; range, 20–81 years; 10 women) who underwent both DWI and dynamic contrast-enhanced MRI between January 2015 and October 2021.

Normalized mean apparent diffusion coefficients (ADCs) and dynamic contrast-enhanced MRI parameters were compared between SM and osseous venous malformations, and between breast cancer and non-small cell lung cancer. Multivariate stepwise logistic regression analyses were performed to identify statistically significant parameters.

Results

Plasma volume and time-to-maximum enhancement were the most statistically significant parameters for differentiating SM from osseous venous malformations, with an area under the receiver operating characteristic curve of 0.962. The normalized mean ADC and peak enhancement values were the most statistically significant parameters for differentiating breast cancer from non-small cell lung cancer, with an area under the curve of 0.924.

Conclusions

Our results highlight the efficacious diagnostic performance of DWI and dynamic contrast-enhanced MRI in distinguishing SM from osseous venous malformations and differentiating SM of various origins.

Introduction

Skull metastasis (SM) is a common form of secondary malignancy observed in 22% of all cancer patients.[1] The primary tumors most frequently associated with SM are breast and lung cancers.[1] SM can lead to the deterioration of patient quality of life due to pain and neurological deficits. Treatment options include resection, antitumor medications (chemotherapy, hormonal therapy, and immunotherapy), and radiation, as determined by the characteristics of metastatic lesions (i.e., size, number, symptoms, growth rate, and drug response).[2] Early detection and characterization are important for the appropriate management of SM and improved chances of long-term survival.

Although computed tomography was the first imaging modality used to evaluate SM at many medical centers, magnetic resonance imaging (MRI) is also useful for SM characterization and detection.[3,4] Nemeth et al. reported improved detection of SM in patients with breast or lung cancers using diffusion-weighted imaging (DWI) compared to conventional sequences (86.7–93.3% and 60%–80% sensitivity for breast and lung cancers, respectively). Recently, advanced MRI sequences, including DWI (or apparent diffusion coefficient [ADC]) and perfusion MRI, have been widely used as indicators to predict the prognosis and determine the treatment efficacy in patients with brain metastases and gliomas.[5–7] However, the characteristics of perfusion MRI findings in SM have not been well-researched.

Dynamic contrast-enhanced (DCE)-MRI is a perfusion MRI method used to assess lesions in the brain, head and neck, and spine.[8–10] Morales et al. reported using DCE-MRI to differentiate vertebral metastases of breast and lung cancers and their mimics, osseous venous malformations (OVMs).[10] However, the characteristics and differences among DCE-MRI parameters between SM and OVM and SM of different origins are yet to be elucidated.

We hypothesized that the DCE-MRI parameters and ADC values would differ between SM and OVM and between SM of different origins, which would be useful for differentiation and informing optimal clinical decision-making. We investigated the characteristics and differences between DCE-MRI parameters and ADC values when comparing SM and OVM, as well as SM of different origins, among patients presenting at our medical center.

Methods

Institutional review board approval and consent exemptions were obtained from the ethics review board of our medical center owing to the retrospective nature of this study. This study was conducted in accordance with the principles and amendments of the Declaration of Helsinki. Data were acquired in compliance with all applicable U.S. Health Insurance Portability and Accountability Act regulations and de-identified before data processing and

analysis. Although not available in public repositories, the data used in this study are available to other researchers upon request.

Patients

Between January 2015 and October 2021, 286 and 333 consecutive patients with suspected SM and OVM, respectively, were identified at our medical center. Among these patients, 52 with SM secondary to breast or non-small-cell lung cancer (NSCLC) and 17 with OVM underwent DCE-MRI to investigate calvarial and possible brain lesions. Seven patients who underwent DCE-MRI after radiotherapy for SM and 14 who underwent scanning using different protocols were excluded from this study.

With respect to OVMs, the initial selection was based on radiological appearance (iso- to hyperintense on T1-weighted imaging [T1WI] and hyperintense on T2WI with enhancement)[11] and proven histology (if available). Cases without histology were included based on the following criteria: the lesion was radiologically stable for >1 year, the case presented with negative positron emission tomography findings, and a "bunch of grapes" appearance was observed upon evaluation.[10,11] One patient with an OVM was excluded because a different scanning protocol was used. Finally, we included and evaluated 31 patients

with SM (median age, 64 years; range, 41–87 years; 29 women) and 16 patients with OVM (median age, 68 years; range, 20–81 years; 10 women).

MRI acquisition

MRI examinations were performed using 1.5-T (n = 37) and 3-T (n = 10) Philips MRI systems (Ingenia, Achieva; Philips Healthcare, Amsterdam, Netherlands). The acquired sequences included axial T1WI and fat-suppressed T2WI, three-dimensional (3D) contrast-enhanced fat-suppressed T1WI, and DWI using echo-planar imaging. DWI was performed with b-values of 0 and 1000 s/mm^2 and the following parameters: repetition time (TR) range, 5,000–9,000 ms; echo time (TE) range, 58–90 ms; number of excitations, 1; slice thickness/gap, 4–5/0–1 mm; field of view, 240 mm × 240 mm; pixel size, 1.5 × 1.5 mm, and three diffusion directions. DCE-MRI was performed using a 3D T1-weighted (3D-T1) fast field echo and the following parameters: TR, 4.8 ms; TE, 2 ms; flip angle, 30°; slice thickness/gap, 5/0 mm; field of view, 200 × 200 mm^2; voxel size/matrix, 1.0 × 1.0 × 5.0 mm^3/240 × 240; number of excitations, 1; number of slices per dynamic scan, 30; temporal resolution, 8.4 s; and total acquisition time, 4 min and 23 s. An intravenous bolus of 20 mL gadobenate dimeglumine contrast (Multihance, Bracco Diagnostics, Milan, Italy) was administered through a peripheral arm vein using a power injector at a flow rate of 5.0 mL/s, followed by a 20-mL saline flush.

DCE-MRI analyses

Quantitative DCE-MRI analyses were conducted using the OleaSphere Permeability Module (Version 3.0; Olea Medical, La Ciotat, France) based on the extended Tofts model,[12] according to which pixel-based parameter maps were calculated from time-intensity curves. Permeability maps were co-registered with 3D fat-suppressed T1WI before measurements. DCE-MRI data were processed with motion artifact correction using rigid-body registration. The arterial input function was calculated automatically using cluster analysis techniques. Deconvolution of the arterial input function was performed using time-insensitive block-circulant singular-value decomposition.[13]

A board-certified radiologist with 9 years of experience in neuroradiology delineated the regions of interest (ROIs) freehand on the permeability maps, including the enhancing components of the tumors, while carefully avoiding cystic, necrotic, or hemorrhagic regions and vessels, which was conducted under the direct supervision of another board-certified radiologist with 13 years of experience in neuroradiology (Figure 1). MRI analyses were performed on the first MRI with DCE-MRI, following the detection of SM or OVM. The largest lesions were observed when multiple lesions were examined. Plasma volume (Vp) and extracellular extravascular volume fractions were automatically calculated and recorded. The

maximum concentration of the contrast agent (peak enhancement) and time-to-maximum enhancement (TME) were automatically calculated and recorded pixel-by-pixel from the time-intensity curves.

ADC analysis

ADC maps were generated using OleaSphere software. ROIs were placed on the solid components of the tumors, as described for DCE-MRI analysis. Three reference ROIs were placed in normal-appearing white matter. The normalized mean ADC (nADCmean) was calculated by dividing the mean ADC value of the tumor by the average mean ADC value of the three reference ROIs (Figure 1).

Statistical analysis

We compared patient age, sex, and the longest diameter between the SM and OVM groups using the Mann–Whitney U and Fisher's exact tests as appropriate. Multivariate stepwise logistic regression analysis using forward stepwise selection was performed to identify the most statistically significant parameters for differentiating between the SM and OVM groups based on quantitative and semiquantitative DCE-MRI parameters and nADCmean values.

Multivariate analysis included variables with two-sided P-values <0.10 in the univariate analysis. The areas under the receiver operating characteristic curves (AUCs) were evaluated for statistically significant parameters using multivariate analysis. The optimal cutoff values for distinguishing between the SM and OVM groups were determined as those that maximized the Youden index (sensitivity + specificity − 1).[14] These analyses were also performed to compare DCE-MRI parameters between SM secondary to breast cancer and NSCLC, and to compare nADCmean between them, using.

Using these cutoff values, the diagnostic performance (sensitivity, specificity, accuracy, and AUC) was calculated for each imaging modality. Two-sided P-values <0.05 were considered statistically significant. All statistical analyses were performed using R software (version 4.1.0; R Foundation for Statistical Computing, Vienna, Austria).

Results

The median patient age did not differ significantly between the SM and OVM groups (64 years [range, 41–87 years] vs. 68 years [20–81 years]) or between the breast cancer and NSCLC groups (65 years [range, 44–87 years] vs. 63 years [41–71 years]). The SM group comprised more women than the OVM group (29/31 vs. 10/16, p = 0.013), as did the breast cancer group compared to the NSCLC group (29/29 vs. 5/7, p = 0.045). No significant difference in the

longest diameter was found between the SM and OVM groups (median 16 mm [range, 7–46 mm] vs. median 11 mm [range, 6–22 mm], p = 0.060).

ADC values and DCE-MRI parameters for SM and OVM

The extravascular volume fraction, Vp, peak enhancement, and TME were significantly higher in the SM group than those in the OVM group. In the multivariate stepwise logistic regression analysis, Vp (odds ratio [OR], 4.26e+27; 95% confidence interval [CI]:1.17e+09–1.55e+46; p = 0.0035) and TME (OR, 1.03; 95% CI:1.00–1.06; p = 0.025) were the most statistically significant parameters for differentiating SM and OVM (Figure 2; Table 1).

ADC values and DCE-MRI parameters for breast cancer and NSCLC

In the univariate analyses, peak enhancement was significantly higher in the breast cancer group than in the NSCLC group, and the nADCmean and TME values were significantly lower (Figures 1 and 3). In the multivariate stepwise logistic regression analysis for differentiating between the breast cancer and NSCLC groups, nADCmean (OR, 0.037; 95%CI, 0.0018–0.75; p = 0.032) and peak enhancement (OR, 1.02; 95%CI:1.00–1.04; p = 0.047) values were the most significant differentiating parameters (Table 2).

Diagnostic performance

The AUCs of the parameters identified in the multivariate analyses and their combinations were as high as 0.962 and 0.924 for differentiating the SM and OVM groups from the breast cancer and NSCLC groups, respectively (Figure 4). The diagnostic performance of each parameter is summarized in Table 3.

Discussion

In the present study, we evaluated the characteristics and differences between DCE-MRI parameters and ADC values between SM and OVM of the skull, as well as SM secondary to breast cancer and NSCLC. Both quantitative (Vp) and semiquantitative (TME) parameters differed significantly between SM and OVM, and ADC values (nADCmean) and semiquantitative parameters (peak enhancement) differed significantly between breast cancer and NSCLC. Using these parameters, the AUCs for differentiating SM, OVM, and SM secondary to breast cancer from NSCLC were 0.962 and 0.924, respectively.

The skull is one of the most frequent sites of secondary malignancies, with primary breast and lung cancers accounting for approximately 70% of SM cases.[3] The prognostic impact of SM may vary according to the specific metastasis site. For example, metastasis to the skull base indicates poor survival.[15] SM may cause severe pain and cosmetic problems and may sometimes lead to neurological deficits due to intracranial tumor growth, thereby greatly deteriorating patient quality of life.[16,17] The treatment strategy for SM was determined after

considering patients' symptoms, tumor site, size, growth rate, and drug responsiveness. Proper radiological characterization of SM is essential for its effective diagnosis and treatment.

In contrast, OVMs are benign vascular lesions, accounting for 10% of benign neoplasms of the skull.[18] OVMs most often occur in middle-aged women.[19] Most OVMs are asymptomatic and grow slowly. However, OVMs can display an aggressive appearance associated with pain and neurological symptoms (i.e., resembling malignancies). Long-term stability and typical radiological appearance are used to confirm OVM diagnosis in clinical practice. However, in situations without reference images or where long-term follow-up is not feasible, radiological differentiation from more urgent conditions (including SM) is critical.

MRI is an essential, noninvasive imaging modality used for diagnosis, biopsy, and surgical/radiation planning, as well as for evaluating therapeutic effects. DWI and DCE-MRI play important roles in diagnosis, glioma grading, differentiation between tumor recurrence and radiation necrosis, and prognostication in neuro-oncology.[5–7,20] Conversely, the role of perfusion MRI in SM is largely unknown, except for a limited number of reports indicating improved detection of arterial spin labeling and slowly progressive enhancement patterns on dynamic susceptibility contrast perfusion MRI.[18,21]

In the present study, DCE-MRI was useful in differentiating SM from OVM. These results are consistent with those of a study by Morales et al.,[10] who reported a significantly

higher Vp in vertebral metastatic cancers with breast or lung origins than in vertebral VMs. The complementary findings of these two studies may reflect the physiology of low plasma volume within the OVM. The significantly longer TME with higher peak enhancement in SM observed in the current study indicated slow and progressive enhancement, consistent with the findings of a study evaluating dynamic susceptibility contrast perfusion MRI.[18]

nADCmean and peak enhancement values differed significantly between the breast cancer and NSCLC groups. The lower nADCmean value in metastases secondary to breast cancer than in NSCLC is consistent with the results of a study on brain metastases by Meyer et al.[22] An important point suggested by the similarities between the present and previous studies of secondary vertebral[10] and brain[22] tumors is that the tumor characteristics observed on DWI and DCE-MRI in the brain and vertebrae can be carried over to the skull lesions. Future studies are needed to investigate the correlations among DCE-MRI parameters, therapeutic response, and prognosis in SM, as these values are already known in metastatic brain tumors.

In addition to the strengths of this study, the study has several limitations. First, it was a retrospective study conducted at a single medical center, thus limiting the generalizability of our findings and the ability to derive causal inferences from the observed results. Second, multiple MRI scanners were used for image acquisition. However, we minimized the resulting risk of heterogeneity in the MRI parameters, which could lead to non-differential

misclassification, by standardizing the vendor and protocol. Third, pathologic confirmation for most OVMs was lacking; however, according to our exclusion criteria, all lesions were stable for >1 year, presented with negative positron emission tomography findings, and presented with a typical radiological appearance. Fourth, the differences in body weights among patients might have affected the contrast enhancement effect and the results of the DCE parameters.

In conclusion, the results of the current study revealed differences in the quantitative and semi-quantitative analyses of Vp and TME when comparing skull metastases with OVMs. Moreover, nADCmean and peak enhancement values were useful for differentiating the origins of skull metastases.

Acknowledgements and Disclosure: The authors have no competing interests to declare.

References

[1] Tofe AJ, Francis MD, Harvey WJ. Correlation of neoplasms with incidence and localization of skeletal metastases: An analysis of 1,355 diphosphonate bone scans. J Nucl Med 1975;16:986-9.

[2] Kotecha R, Angelov L, Barnett GH, et al. Calvarial and skull base metastases: Expanding the clinical utility of gamma Knife surgery. J Neurosurg 2014;121(Suppl):91-101.

[3] Mitsuya K, Nakasu Y, Horiguchi S, et al. Metastatic skull tumors: MRI features and a new conventional classification. J Neurooncol 2011;104:239-45.

[4] Nemeth AJ, Henson JW, Mullins ME, Gonzalez RG, Schaefer PW. Improved detection of skull metastasis with diffusion-weighted MR imaging. AJNR Am J Neuroradiol 2007;28:1088-92.

[5] Kerkhof M, Ganeff I, Wiggenraad RGJ, et al. Clinical applicability of and changes in perfusion MR imaging in brain metastases after stereotactic radiotherapy. J Neurooncol 2018;138:133-9.

[6] Nguyen TB, Cron GO, Perdrizet K, et al. Comparison of the diagnostic accuracy of DSC- and dynamic contrast-enhanced MRI in the preoperative grading of astrocytomas. AJNR Am J Neuroradiol 2015;36:2017-22.

[7] Choi SH, Jung SC, Kim KW, et al. Perfusion MRI as the predictive/prognostic and pharmacodynamic biomarkers in recurrent malignant glioma treated with bevacizumab: A systematic review and a time-to-event meta-analysis. J Neurooncol 2016;128:185-94.

[8] Jung BC, Arevalo-Perez J, Lyo JK, et al. Comparison of glioblastomas and brain metastases using dynamic contrast-enhanced perfusion MRI. J Neuroimaging 2016;26:240-6.

[9] Ota Y, Liao E, Capizzano AA, et al. Diagnostic role of diffusion-weighted and dynamic contrast-enhanced perfusion MR imaging in paragangliomas and schwannomas in the head and neck. AJNR Am J Neuroradiol 2021;42:1839-46.

[10] Morales KA, Arevalo-Perez J, Peck KK, Holodny AI, Lis E, Karimi S. Differentiating atypical hemangiomas and metastatic vertebral lesions: The role of T1-weighted dynamic contrast-enhanced MRI. AJNR Am J Neuroradiol 2018;39:968-73.

[11] Gomez CK, Schiffman SR, Bhatt AA. Radiological review of skull lesions. Insights Imaging 2018;9:857-82.

[12] Tofts PS. Modeling tracer kinetics in dynamic Gd-DTPA MR imaging. J Magn Reson Imaging 1997;7:91-101.

[13] Mouridsen K, Christensen S, Gyldensted L, Ostergaard L. Automatic selection of arterial input function using cluster analysis. Magn Reson Med 2006;55:524-31.

[14] Youden WJ. Index for rating diagnostic tests. Cancer 1950;3:32-5.

[15] Laigle-Donadey F, Taillibert S, Martin-Duverneuil N, Hildebrand J, Delattre JY. Skull-base metastases. J Neurooncol 2005;75:63-9.

[16] Michael CB, Gokaslan ZL, DeMonte F, McCutcheon IE, Sawaya R, Lang FF. Surgical resection of calvarial metastases overlying dural sinuses. Neurosurgery 2001;48:745-54.

[17] Nayak L, Abrey LE, Iwamoto FM. Intracranial dural metastases. Cancer 2009;115:1947-53.

[18] Pons Escoda A, Naval Baudin P, Mora P, et al. Imaging of skull vault tumors in adults. Insights Imaging 2020;11:23.

[19] Bastug D, Ortiz O, Schochet SS. Hemangiomas in the calvaria: Imaging findings. AJR Am J Roentgenol 1995;164:683-7.

[20] Chuang MT, Liu YS, Tsai YS, Chen YC, Wang CK. Differentiating radiation-induced necrosis from recurrent brain tumor using MR perfusion and spectroscopy: A meta-analysis. PLoS One 2016;11:e0141438.

[21] Ryu KH, Baek HJ, Cho SB, et al. Skull metastases detecting on arterial spin labeling perfusion: Three case reports and review of literature. Medicine 2017;96:e8432.

[22] Meyer HJ, Fiedler E, Kornhuber M, Spielmann RP, Surov A. Comparison of diffusion-weighted imaging findings in brain metastases of different origin. Clin Imaging 2015;39:965-9.

Figure captions

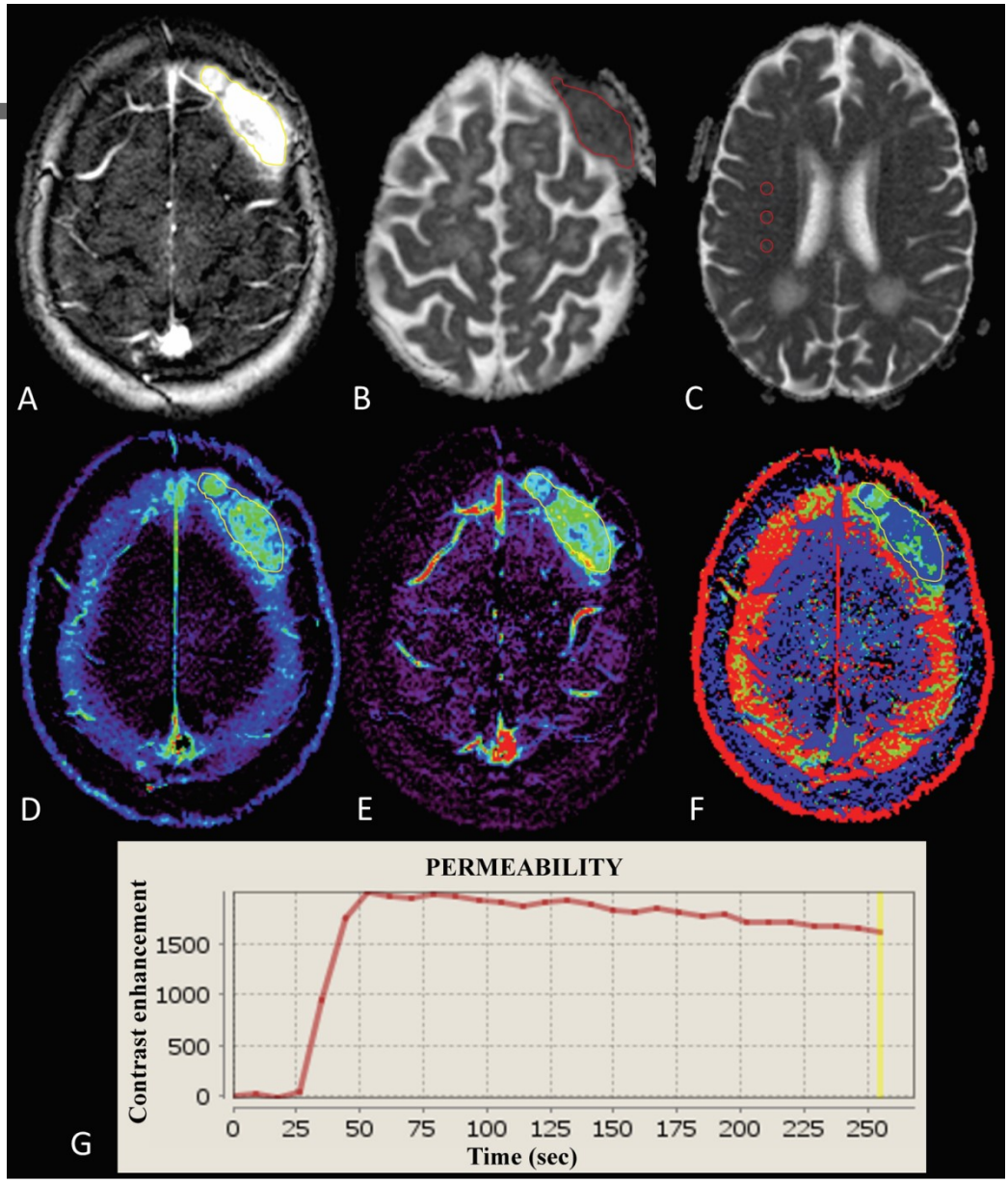

Figure 1. Imaging findings in a 67-year-old woman with newly observed skull metastasis (SM) secondary to breast cancer occurring in the left frontal bone.

Permeability mapping showing a homogeneously enhanced mass (A). The mass showed low signal intensity on the apparent diffusion coefficient (ADC) map with a normalized mean ADC

value of 0.85 (B). Three reference regions of interest were placed in the normal-appearing white matter on the ADC map (C). Extracellular extravascular volume fraction, plasma volume, and time-to-maximum enhancement maps are shown (D–F, respectively). The time-intensity curve indicates a high peak with a slow washout (G). sec = second.

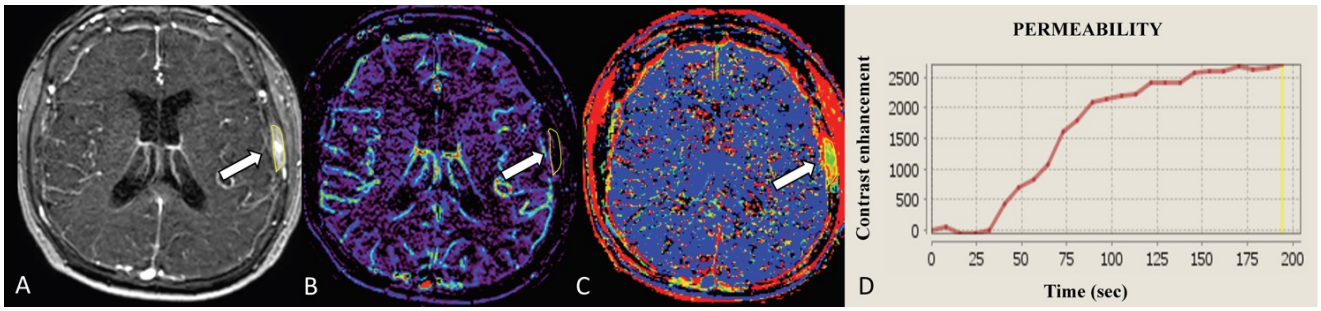

Figure 2. Imaging findings in a 74-year-old woman with an osseous venous malformation in the left parietal bone (arrows).

Permeability mapping showing a heterogeneously enhanced mass (A). The plasma volume and time-to-maximum enhancement values are 0.01 and 102.8, respectively (B, C). The time-intensity curve shows enhancement with a high plateau peak (D). sec = second.

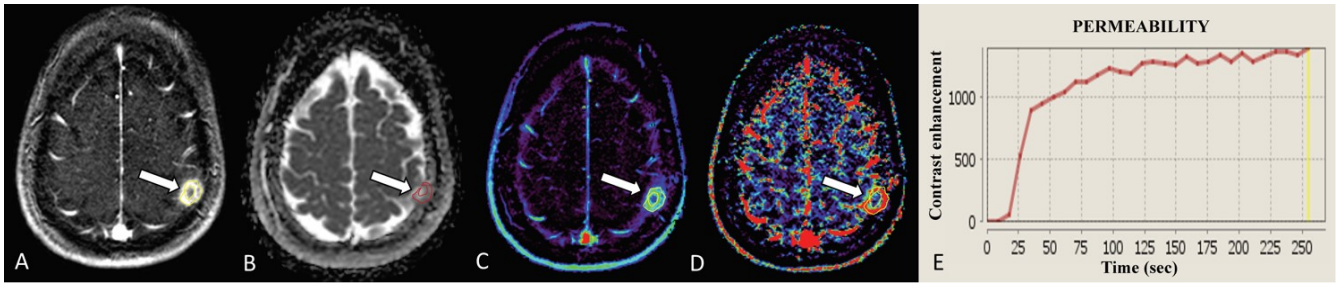

Figure 3. Imaging findings in a 70-year-old woman with a newly observed skull metastasis secondary to non-small cell lung cancer in the left parietal bone (arrows).

Permeability mapping showing a heterogeneously enhanced mass (A). The mass shows low signal intensity on apparent diffusion coefficient (ADC) mapping, with a normalized mean ADC of 1.56 (B). The extracellular extravascular volume fraction and peak enhancement values are 0.42 and 151.06, respectively (C, D). The time-intensity curve shows an enhancement with a high and persistent peak (E). sec = second.

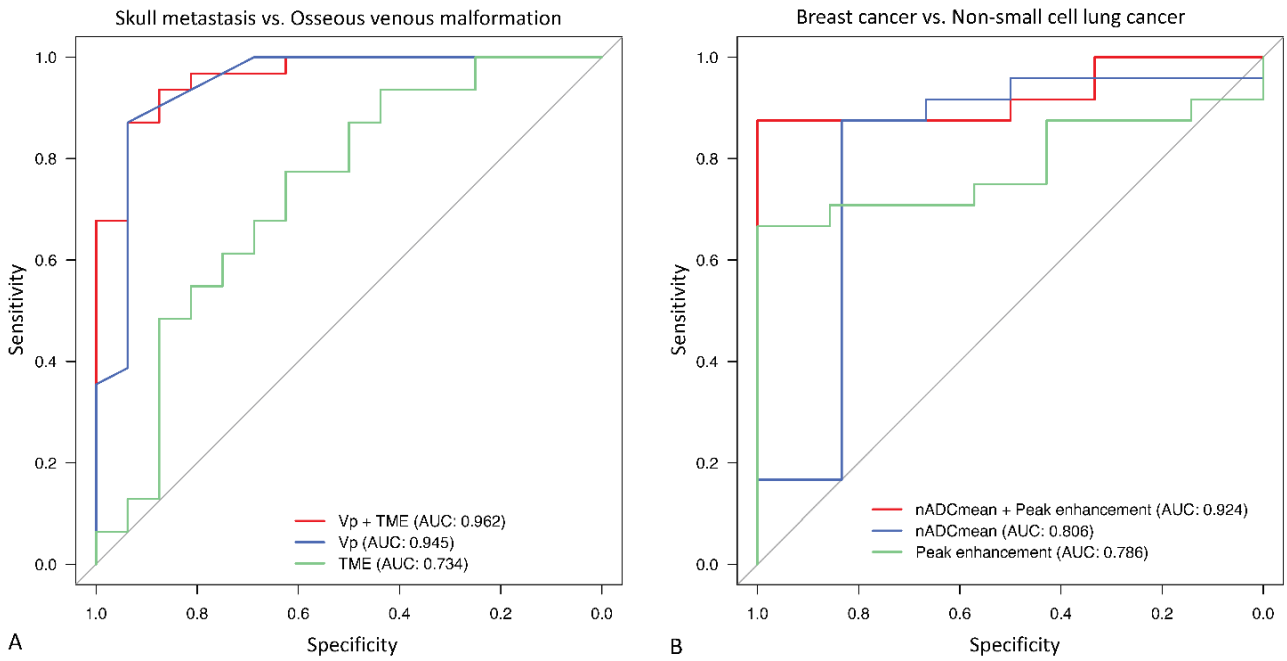

Figure 4. Receiver operating characteristic curves.

The areas under the curve (AUCs) for plasma volume (Vp) + time-to-maximum enhancement (TME) (combined, red), Vp (blue), and TME (green) for differentiating skull metastasis and osseous venous lesions were 0.962, 0.945, and 0.734, respectively (A). The AUCs for normalized mean apparent diffusion coefficient (ADC) (nADCmean) + peak enhancement (combined, red), nADCmean (blue), and peak enhancement (green) values for differentiating

between the breast cancer and non-small cell lung cancer groups were 0.924, 0.806, and 0.786, respectively (B).

Tables

Table 1. ADC values and DCE-MRI parameters of osseous venous malformation and skull metastases

	Venous malformation (16 patients)	Skull metastasis (31 patients)	Univariate analysis (OR [95% confidence intervals])	P-value	Multivariate analysis (OR [95% confidence intervals])	P-value
Normalized mean ADC[a]	1.45 (0.96–2.05)	1.17 (1.05–1.46)	0.38 [0.12–1.22]	0.11		
Quantitative values[a]						

Vp	<0.005 (<0.005–0.010)	0.090 (0.050–0.14)	7.69e+25 [2.40e+09–2.46e+42]	0.0021*	4.26e+27 [1.17e+09–1.55e+46]	0.0035*
Extravascular volume fraction	0.14 (0.025–0.55)	0.42 (0.30–0.70)	16.90 [1.37–208.0]	0.027*	Removed	
Semiquantitative values[a]						
Peak enhancement	5.86 (2.02–30.02)	198.54 (142.49–269.59)	1.02 [1.01–1.03]	<0.001*	Removed	
TME	88.53 (51.11–132.27)	146.71 (105.07–181.42)	1.02 [1.00–1.03]	0.0087*	1.03 [1.00–1.06]	0.025*

ADC = apparent diffusion coefficient; DCE = dynamic contrast-enhanced; OR = odds ratio;

Vp = plasma volume; TME = time-to-maximum enhancement

[a]Median (interquartile range) *P < 0.05

Table 2. ADC values and DCE-MRI parameters of skull metastases of breast cancer and NSCLC

	Breast cancer (24 patients)	NSCLC (7 patients)	Univariate analysis (OR [95% confidence intervals])	P value	Multivariate analysis (OR [95% confidence intervals])	P value
Normalized mean ADC[a]	1.13 (1.03–1.24)	1.56 (1.19–1.81)	0.045 [0.0028–0.72]	0.028*	0.037 [0.0018–0.75]	0.032*
Quantitative values[a]						
Vp	0.093 (0.058–	0.050 (0.015–	1.37e+08 [0.12–	0.079		

	0.16)	0.070)	1.60e+17]			
Extravascular volume fraction	0.41 (0.30–0.74)	0.42 (0.32–0.54)	2.04 [0.057–72.7]	0.70		
Semiquantitative values[a]						
Peak enhancement	240.26 (151.94–274.44)	151.06 (75.61–162.51)	1.01 [1.00–1.03]	0.029*	1.02 [1.00–1.04]	0.047*
TME	126.07 (97.14–161.28)	184.22 (177.8–192.25)	0.97 [0.94–0.996]	0.029*	Removed	

ADC = apparent diffusion coefficient; DCE = dynamic contrast-enhanced; NSCLC = non-small cell lung cancer; OR = odds ratio; Vp = plasma volume; TME = time-to-maximum enhancement

[a]Median (interquartile range) *P < 0.05

Table 3. Diagnostic performance of nADCmean and DCE-MRI parameters

	SM vs. OVM		Breast cancer vs. NSCLC	
	Vp	TME	nADCmean	Peak enhancement
Cutoff	0.020	104.85	1.405	198.54
Sensitivity	0.871	0.774	0.875	0.667
Specificity	0.938	0.625	0.833	1
AUC	0.945	0.734	0.806	0.786

nADCmean = normalized mean ADC; DCE = dynamic contrast-enhanced; SM = skull metastasis; OVM = osseous venous malformation; NSCLC = non-small cell lung cancer; Vp = plasma volume; TME = time-to-maximum enhancement; AUC = Area under the receiver operating characteristic curve